

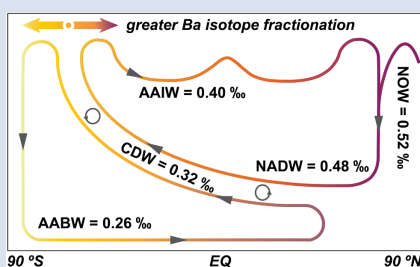
High latitude controls on dissolved barium isotope distributions in the global ocean

Y. Yu^{1*}, R.C. Xie^{1,2}, M. Gutjahr¹, G. Laukert^{1,3,4}, Z. Cao⁵, E. Hathorne¹, C. Siebert¹,
G. Patton⁶, M. Frank¹



<https://doi.org/10.7185/geochemlet.2242>

Abstract



The high latitude regions play a key role in regulating the marine biogeochemical cycling of barium (Ba) and the pre-formed Ba isotope compositions in the global ocean. In this study, we present 17 new depth profiles of dissolved Ba concentrations ([Ba]) and isotope compositions ($\delta^{138}\text{Ba}$) from the high latitude Atlantic, Pacific and Southern Oceans to trace the ventilation of deep waters in the Southern Ocean and their subsequent transport throughout the global ocean. Our data reveal how biogeochemical processes in the Southern Ocean generate distinct $\delta^{138}\text{Ba}$ signatures of upper ocean water masses, and that large scale ocean circulation constrains the meridional gradient of $\delta^{138}\text{Ba}$ distributions in the deep Atlantic Ocean. The significant increase in [Ba] of deep waters in the North Pacific is mainly achieved through dissolution of sinking particles which adds a $\delta^{138}\text{Ba}$ signal comparable to the deep Pacific Ocean.

Received 5 July 2022 | Accepted 28 November 2022 | Published 21 December 2022

Introduction

Barium (Ba) is a bio-intermediate element in the ocean, whose dissolved concentrations ([Ba]) in the water column have a nutrient-like depth profile with a [Ba] depletion in the upper ocean resulting from removal *via* marine particles (*e.g.*, barite) and [Ba] enrichment at depth due to particulate matter decomposition and remineralisation (Lea and Boyle, 1991). Recent studies presenting novel dissolved Ba isotope compositions ($\delta^{138}\text{Ba}$) have provided additional insights into the processes driving the oceanic cycling of Ba (*e.g.*, Horner *et al.*, 2015; Cao *et al.*, 2016; Hsieh and Henderson, 2017). In the uppermost water column, Ba isotope fractionation is likely induced by preferential adsorption of the light isotopes onto biogenic particles (Cao *et al.*, 2020). Although laboratory experiments of adsorption to silica hydrogel exhibited Ba isotope fractionation in the opposite direction, with heavy Ba isotopes being preferentially adsorbed (van Zuilen *et al.*, 2016), field observations consistently reveal lighter isotope enrichment in surface water particles (Horner *et al.*, 2017; Cao *et al.*, 2020). During sinking and decomposition of these particles, barite formation with a preference for the assimilation of light isotopes (von Allmen *et al.*, 2010) leads to high dissolved $\delta^{138}\text{Ba}$ values in subsurface seawater (Horner *et al.*, 2015; Bates *et al.*, 2017). In contrast, $\delta^{138}\text{Ba}$ values of deep waters appear to be mainly controlled by barite dissolution and large scale ocean circulation (Hsieh and Henderson, 2017).

Given that the oceanic residence time of dissolved Ba (~3.5 to 5 kyr; Rahman *et al.*, 2022) is longer than the global ocean mixing time, but short enough to prevent complete homogenisation, studies have focused on the importance of advection and mixing on determining dissolved $\delta^{138}\text{Ba}$ within water masses in the deep Atlantic Meridional Overturning Circulation (AMOC; Bates *et al.*, 2017; Hsieh and Henderson, 2017). The distribution of deep water $\delta^{138}\text{Ba}$ is overall consistent with two end member mixing between North Atlantic Deep Water (NADW) and Antarctic Bottom Water (AABW). However, the lack of $\delta^{138}\text{Ba}$ data from high latitude regions where these water masses form results in uncertain end member $\delta^{138}\text{Ba}$ signatures. Additionally, despite several studies in the Atlantic Ocean, the stable Ba isotope distribution in global seawater, in particular in the Indo-Pacific, remains largely unconstrained. The still poor spatial coverage of available data has so far prevented a robust identification of the mechanisms controlling the distribution of dissolved Ba isotopes in the global ocean.

Here, we examine the spatial and vertical distribution of $\delta^{138}\text{Ba}$ and [Ba] in 17 new water depth profiles from the high latitude Atlantic, Pacific and Southern Oceans (Fig. 1). These data reveal how NADW and AABW acquire their respective Ba isotope signatures in the polar and subpolar regions. In combination with previously reported low and mid-latitude $\delta^{138}\text{Ba}$ profiles (Horner *et al.*, 2015; Bates *et al.*, 2017; Hsieh and

1. GEOMAR Helmholtz Centre for Ocean Research, Kiel, Germany
2. School of Oceanography, Shanghai Jiao Tong University, Shanghai, China
3. Department of Oceanography, Dalhousie University, Halifax, Canada
4. Woods Hole Oceanographic Institution, Woods Hole, USA
5. State Key Laboratory of Marine Environmental Science and College of Ocean and Earth Sciences, Xiamen University, Xiamen, China
6. PCIGR, Department of Earth, Ocean and Atmospheric Sciences, Vancouver, Canada

* Corresponding author (email: yyu@geomar.de)



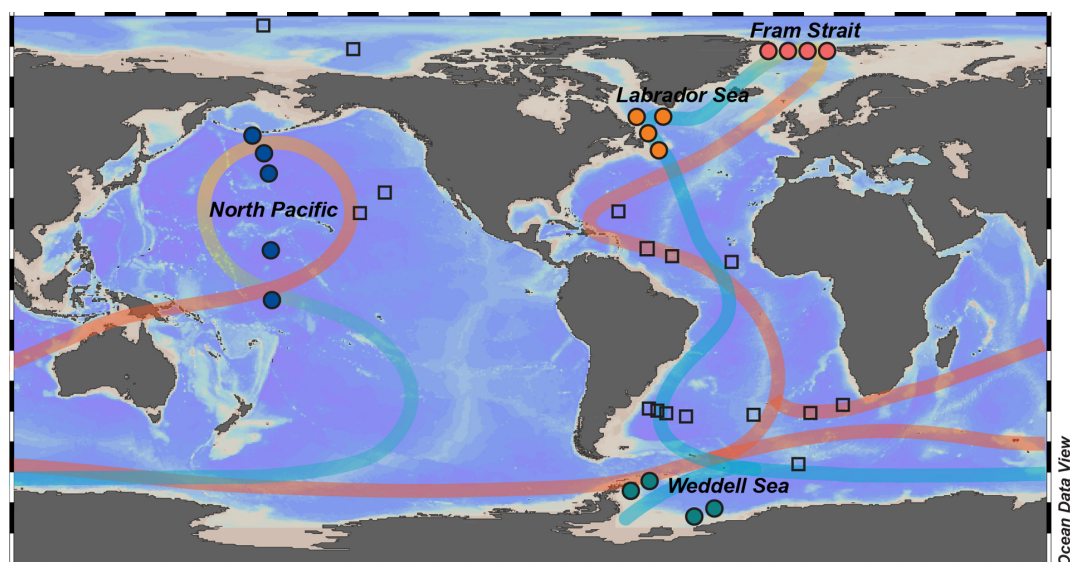


Figure 1 Simplified global overturning circulation with locations of seawater profile stations of this study (coloured circles). Open squares denote published profiles (Horner *et al.*, 2015; Bates *et al.*, 2017; Hsieh and Henderson, 2017; Bridgestock *et al.*, 2018; Geyman *et al.*, 2019; Whitmore *et al.*, 2022). Produced using Ocean Data View (Schlitzer, 2022).

Henderson, 2017; Bridgestock *et al.*, 2018; Geyman *et al.*, 2019), we are now able to better constrain Ba isotope fractionation in the upper ocean and to obtain a more complete picture of the $\delta^{138}\text{Ba}$ systematics within the global overturning circulation.

Ba Isotope Fractionation in the Upper Ocean

Seawater samples for dissolved [Ba] and $\delta^{138}\text{Ba}$ were measured at GEOMAR, Kiel, applying methods detailed in Yu *et al.* (2020) and the Supplementary Information. The depth profiles of $\delta^{138}\text{Ba}$ from the Fram Strait, the Labrador Sea and the Weddell Sea are shown together with two low and mid-latitude Atlantic $\delta^{138}\text{Ba}$

profiles, overlain by [Ba] data in Figure 2. The samples in the surface and subsurface Weddell Sea have relatively high [Ba] ($\sim 90 \text{ nmol kg}^{-1}$) and low $\delta^{138}\text{Ba}$ ($\sim 0.3 \text{ ‰}$), suggesting that the southward intrusion of Circumpolar Deep Water (CDW) was associated with little Ba depletion and isotope fractionation relative to the AABW end member. Previous studies have suggested that the low availability of light and micronutrients (e.g., iron) limits phytoplankton growth in the upper Weddell Sea despite the large inventory of major nutrients available for phytoplankton growth (Sunda and Huntsman, 1997). The minor Ba isotope fractionation in the upper Weddell Sea, as a result of limited barite formation, is consistent with the relatively low productivity of this well known high nutrient low chlorophyll (HNLC) region. The strong upwelling of CDW from below, on

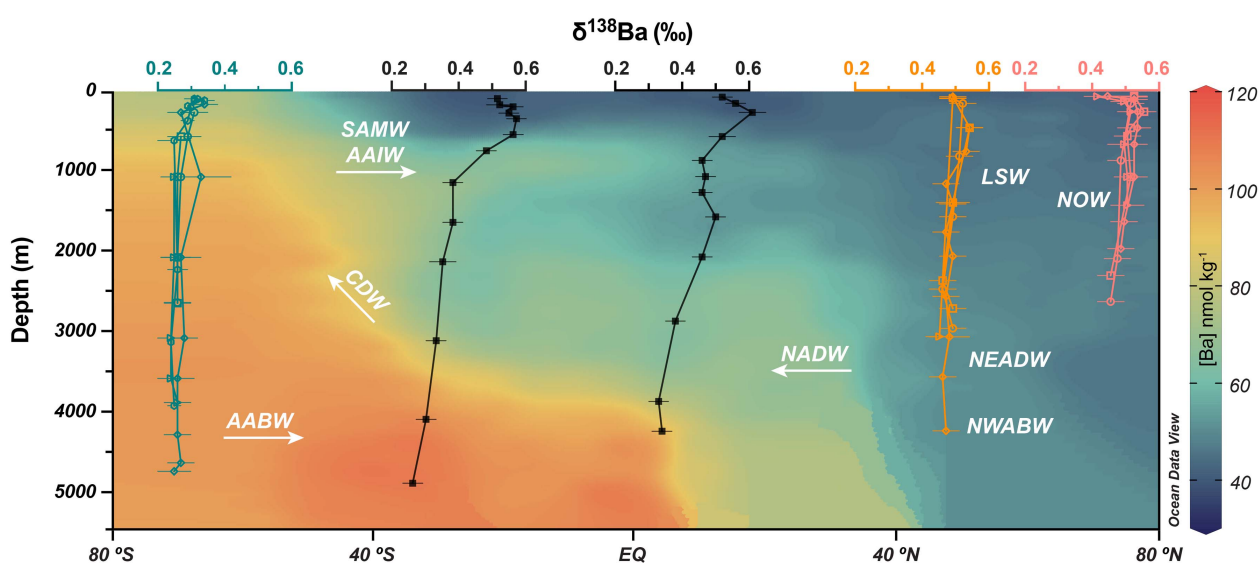


Figure 2 Depth profiles of dissolved $\delta^{138}\text{Ba}$ in the Weddell Sea (green), the Labrador Sea (orange), the Fram Strait (pink), and the low and mid-latitude Atlantic Ocean (black, Bates *et al.*, 2017). Dissolved [Ba] data are from the GEOTRACES intermediate data product 2017 (Schlitzer *et al.*, 2018) and this study. SAMW, Subantarctic Mode Water; AAIW, Antarctic Intermediate Water; CDW, Circumpolar Deep Water; AABW, Antarctic Bottom Water; NADW, North Atlantic Deep Water; LSW, Labrador Sea Water; NEADW, Northeast Atlantic Deep Water; NWABW, Northwest Atlantic Bottom Water; NOW, Northern Overflow Water. Produced using Ocean Data View (Schlitzer, 2022).

the other hand, further diminishes the degree of Ba isotope fractionation, resulting in a homogenous water column $\delta^{138}\text{Ba}$ signature that is indistinguishable from that of CDW.

In contrast, the upwelled CDW that moves northwards by Ekman transport undergoes strong Ba isotope fractionation due to high diatom productivity resulting in Ba adsorption to particles in the surface and barite precipitation at intermediate depths (Horner *et al.*, 2015; Cao *et al.*, 2016). As Subantarctic Mode Water (SAMW) and Antarctic Intermediate Water (AAIW) flow northwards from the Subantarctic Zone, surface and subsurface dissolved $\delta^{138}\text{Ba}$ values increase from ~ 0.3 to ~ 0.6 ‰ and ultimately reach high $\delta^{138}\text{Ba}$ values observed in the Labrador Sea and the Fram Strait (Fig. 2). This meridional upper ocean contrast along the upper limb of the AMOC reflects the combined effects of biologically mediated isotope fractionation at high southern latitudes and the role of large scale ocean circulation.

In the tropical and subtropical Pacific Ocean, [Ba] and $\delta^{138}\text{Ba}$ exhibit larger gradients between the surface and deep waters than those in the Atlantic Ocean (Fig. 3). The stronger Ba depletion ($\sim 30 \text{ nmol kg}^{-1}$) and associated greater Ba isotope fractionation (~ 0.62 ‰) likely result from the weak vertical mixing in the North Pacific Gyre (Emery and Dewar, 1982), allowing more time for Ba removal associated with particle adsorption and barite formation in the upper ocean. In contrast, upper ocean Ba isotope fractionation becomes less pronounced northwards, where [Ba] slightly increases in the sub-Arctic Pacific (Fig. 3). These less fractionated Ba isotope signatures reflect the limited biological productivity of the HNLC region in the upper sub-Arctic Pacific, similar to that of the Weddell Sea.

Ba Isotope Distribution in the Deep Ocean

The [Ba] and $\delta^{138}\text{Ba}$ signatures pre-formed in the surface are subducted by deep water formation at high latitudes (*e.g.*, Weddell Sea and Labrador Sea). Due to the vigorous circulation of the Weddell Sea, four depth profiles in the southern and western Weddell Sea (Fig. S-2) are indistinguishable from each other in their $\delta^{138}\text{Ba}$ values, which defines the end member Ba isotope

composition of AABW at 0.26 ± 0.03 ‰. In the Labrador Sea, Labrador Sea Water (LSW), Northeast Atlantic Deep Water (NEADW) and Northwest Atlantic Bottom Water (NWABW) have essentially invariant $\delta^{138}\text{Ba}$ values and thus define the end member Ba isotope composition of NADW as 0.48 ± 0.05 ‰ (Fig. S-2).

The distinctive Ba isotope signatures of deep waters originating in the Weddell Sea and those in the high latitude North Atlantic (*i.e.* Nordic Seas and Labrador Sea) constrain the meridional gradient of Ba isotope compositions in the deep ocean. The deep ocean $\delta^{138}\text{Ba}$ and [Ba] data obtained here are compiled with previously reported profiles in a $\delta^{138}\text{Ba}$ against $1/[\text{Ba}]$ plot (Fig. 4). The high latitude dissolved $\delta^{138}\text{Ba}$ and $1/[\text{Ba}]$ data display a linear correlation (black dashed line) suggesting conservative mixing between the Northern Overflow Waters (NOW) with low [Ba] and high $\delta^{138}\text{Ba}$ and AABW characterised by elevated [Ba] and low $\delta^{138}\text{Ba}$. The $\delta^{138}\text{Ba}$ signature of NADW (0.48 ± 0.05 ‰) in the Labrador Sea is only slightly lower than that of NOW (0.52 ± 0.07 ‰), and a clear $\delta^{138}\text{Ba}$ - $1/[\text{Ba}]$ mixing relationship is observed between NOW, NADW and the waters from the deep subtropical North Atlantic (Fig. 4). This suggests that the pre-formed Ba isotope signature of NOW in the Fram Strait represents the northernmost end member of the global deep ocean mixing trend, which is modified along its pathway to the production sites of NADW due to the entrainment of Lower Deep Water (LDW) at greater depth.

It could be argued that the coupled changes in $1/[\text{Ba}]$ and $\delta^{138}\text{Ba}$ can also be explained by a regeneration model, in which light Ba isotopes are progressively regenerated from sinking particles driving the deep oceans towards a higher [Ba] and lower $\delta^{138}\text{Ba}$ values. The results of such a model are shown in Figure 4 and the Supplementary Information. As outlined by Bridgestock *et al.* (2018) and Hsieh and Henderson (2017), the continuous addition of Ba from sinking particles along the southward flow of deep Atlantic water masses is unlikely to generate significant deviations from the mixing line, confirmed by the similarity with the regeneration model (Fig. 4). In contrast, some low and mid-latitude data clearly deviate towards heavier $\delta^{138}\text{Ba}$ values, which requires the involvement of a third mixing end member. Hsieh *et al.* (2021) presented Ba isotope measurements

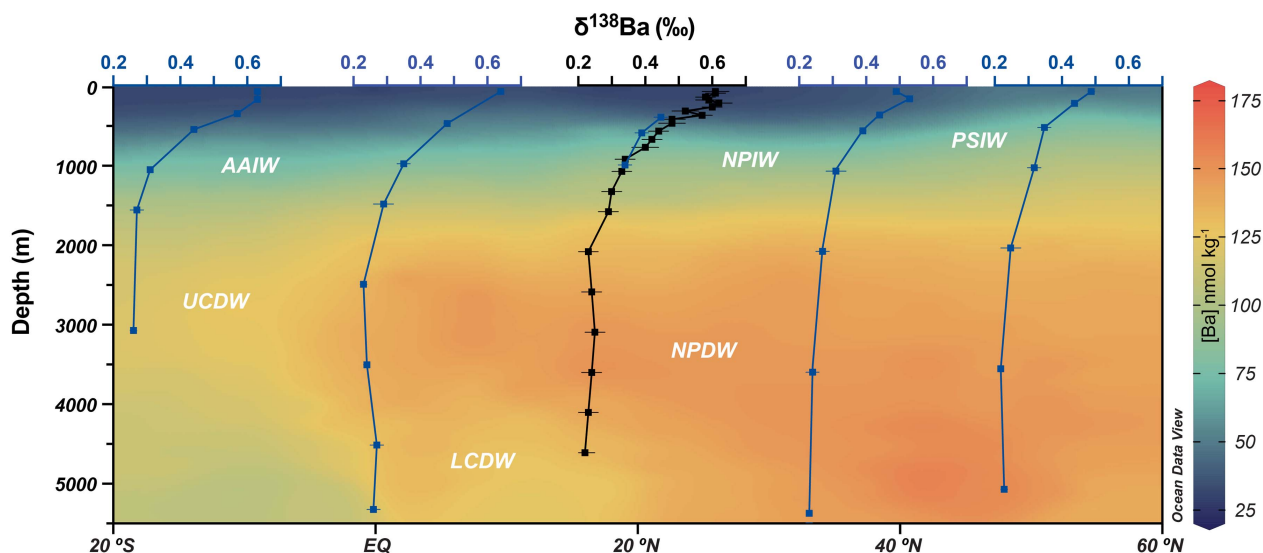


Figure 3 Depth profiles of dissolved $\delta^{138}\text{Ba}$ in the Pacific Ocean (blue). The depth profile of $\delta^{138}\text{Ba}$ in the mid-latitude North Pacific (SAFE station, black) is from Geyman *et al.* (2019). Dissolved [Ba] data are from the GEOTRACES intermediate data product 2017 (Schlitzer *et al.*, 2018) and this study. UCDW, Upper Circumpolar Deep Water; LCDW, Lower Circumpolar Deep Water; NPIW, North Pacific Intermediate Water; NPDIW, North Pacific Deep Water; PSIW, Pacific Subpolar Intermediate Water. Produced using Ocean Data View (Schlitzer, 2022).

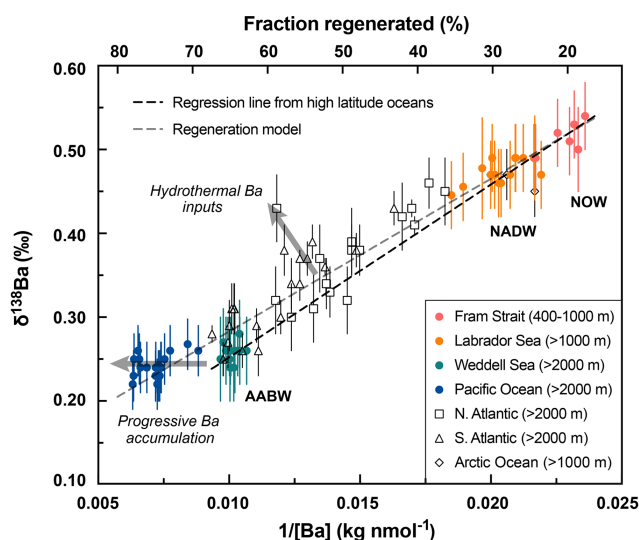


Figure 4 Deep ocean mixing line (black dashed line; data from this study) of $\delta^{138}\text{Ba}$ against $1/[\text{Ba}]$ and results of a regeneration model assuming a pre-formed $[\text{Ba}]$ of 35 nmol kg^{-1} and a $\delta^{138}\text{Ba}$ value of 0.62 ‰ (grey dashed line). Literature dissolved $\delta^{138}\text{Ba}$ and $[\text{Ba}]$ data (black) are from Horner *et al.* (2015), Bates *et al.* (2017), Hsieh and Henderson (2017), Bridgestock *et al.* (2018), Geyman *et al.* (2019), and Whitmore *et al.* (2022). The potential impacts of hydrothermal Ba input in the Atlantic and progressive Ba accumulation in the deep Pacific are denoted by bold light grey arrows.

in several hydrothermal vent fluids and suggested that significant inputs of hydrothermal Ba contribute significant amounts of Ba with high $\delta^{138}\text{Ba}$ to the deep ocean, which causes deviations from the high latitude end member mixing line and the regeneration model (Fig. 4). By excluding these deep water masses that are potentially influenced by hydrothermal inputs, a conservative mixing model was applied to quantify the variability of dissolved $\delta^{138}\text{Ba}$ not related to conservative mixing in the low and mid-latitude Atlantic Ocean. However, the lack of deviations of the $\delta^{138}\text{Ba}$ values from conservative mixing indicates any effects of particle regeneration are within analytical uncertainties and non-conservative contributions originating from biogeochemical cycling are small in this case (Fig. S-3 and the Supplementary Information).

In the deep Pacific, water masses below $\sim 2000 \text{ m}$ depth are characterised by light Ba isotope compositions indistinguishable from those of the deep Weddell Sea, though with significantly higher $[\text{Ba}]$ (Fig. 4). A higher fraction of regenerated Ba in the deep Pacific would be expected to cause deviations from the observed mixing relationship at higher $[\text{Ba}]$ accompanied by slightly elevated $\delta^{138}\text{Ba}$ values (Fig. 4). The substantially high proportion of regenerated Ba ($\sim 75 \%$) in the deep Pacific, along with the high Ba ‘utilisation’ ($\sim 70 \%$) in the upper North Pacific indicated by Hsieh and Henderson (2017), demonstrates that biogeochemical Ba cycling plays a more important role in regulating the deep Pacific $\delta^{138}\text{Ba}$ signatures than in the Atlantic Ocean. In contrast to the regeneration model, the uniformity of deep water $\delta^{138}\text{Ba}$ signatures in the Southern Ocean and the North Pacific indicates little or no Ba isotope fractionation during progressive accumulation of Ba along the conveyor belt in the deep Pacific. A homogeneity similar to that of $\delta^{138}\text{Ba}$ signatures is also observed in the dissolved $\delta^{30}\text{Si}$ and $\delta^{114}\text{Cd}$ distribution in the deep Pacific, where both isotope values are indistinguishable from those of the deep Southern Ocean (de Souza *et al.*, 2014; Janssen *et al.*, 2017; Xie *et al.*, 2019). Using a simple mass balance calculation developed for stable Cd

isotopes by Janssen *et al.* (2017), the net accumulated Ba originating from dissolution of sinking particles in the deep North Pacific is characterised by an average $\delta^{138}\text{Ba}$ value of $0.22 \pm 0.24 \text{ ‰}$ (Supplementary Information), which is consistent with the deep Pacific $\delta^{138}\text{Ba}$ signature of $0.25 \pm 0.04 \text{ ‰}$. Pacific deep water $\delta^{138}\text{Ba}$ thus reflects a mixture of biogeochemical Ba cycling and large scale ocean circulation considering its similarity to AABW ($0.26 \pm 0.03 \text{ ‰}$). This new detailed view of the oceanic Ba cycle will facilitate the use of Ba concentrations and stable isotopes as tracers for ocean circulation globally and for biogeochemical processes in specific regions.

Acknowledgements

The authors would like to thank Jutta Heinze and Ana Kolevica for their support in the laboratory. Many thanks to the captains, crews, and participants of RV *Sonne* cruise SO-264, RV *Maria S. Merian* cruises MSM-39, MSM-45, RV *Polarstern* cruises PS-80, PS-111, and PS-118 for seawater sampling, particularly Huang. GL acknowledges financial support by the Ocean Frontier Institute through an award from the Canada First Research Excellence Fund. RCX was supported by a German DFG grant (project number 432469432). The China Scholarship Council is acknowledged for financial support of YY during this study.

Editor: Gavin Foster

Additional Information

Supplementary Information accompanies this letter at <https://www.geochemicalperspectivesletters.org/article2242>.



© 2022 The Authors. This work is distributed under the Creative Commons Attribution Non-Commercial No-Derivatives 4.0

License, which permits unrestricted distribution provided the original author and source are credited. The material may not be adapted (remixed, transformed or built upon) or used for commercial purposes without written permission from the author. Additional information is available at <https://www.geochemicalperspectivesletters.org/copyright-and-permissions>.

Cite this letter as: Yu, Y., Xie, R.C., Gutjahr, M., Laukert, G., Cao, Z., Hathorne, E., Siebert, C., Patton, G., Frank, M. (2022) High latitude controls on dissolved barium isotope distributions in the global ocean. *Geochem. Persp. Let.* 24, 22–26. <https://doi.org/10.7185/geochemlet.2242>

References

- BATES, S.L., HENDRY, K.R., PRYER, H.V., KINSLEY, C.W., PYLE, K.M., WOODWARD, E.M.S., HORNER, T.J. (2017) Barium isotopes reveal role of ocean circulation on barium cycling in the Atlantic. *Geochimica et Cosmochimica Acta* 204, 286–299. <https://doi.org/10.1016/j.gca.2017.01.043>
- BRIDGESTOCK, L., HSIEH, Y.-T., PORCELLI, D., HOMOKY, W.B., BRYAN, A., HENDERSON, G.M. (2018) Controls on the barium isotope compositions of marine sediments. *Earth and Planetary Science Letters* 481, 101–110. <https://doi.org/10.1016/j.epsl.2017.10.019>
- CAO, Z., SIEBERT, C., HATHORNE, E.C., DAL, M., FRANK, M. (2016) Constraining the oceanic barium cycle with stable barium isotopes. *Earth and Planetary Science Letters* 434, 1–9. <https://doi.org/10.1016/j.epsl.2015.11.017>
- CAO, Z., LI, Y., RAO, X., YU, Y., HATHORNE, E.C., SIEBERT, C., DAL, M., FRANK, M. (2020) Constraining barium isotope fractionation in the upper water column of the South China Sea. *Geochimica et Cosmochimica Acta* 288, 120–137. <https://doi.org/10.1016/j.gca.2020.08.008>

- DE SOUZA, G.F., SLATER, R.D., DUNNE, J.P., SARMIENTO, J.L. (2014) Deconvolving the controls on the deep ocean's silicon stable isotope distribution. *Earth and Planetary Science Letters* 398, 66–76. <https://doi.org/10.1016/j.epsl.2014.04.040>
- EMERY, W.J., DEWAR, J.S. (1982) Mean temperature-salinity, salinity-depth and temperature-depth curves for the North Atlantic and the North Pacific. *Progress in Oceanography* 11, 219–305. [https://doi.org/10.1016/0079-6611\(82\)90015-5](https://doi.org/10.1016/0079-6611(82)90015-5)
- GEYMAN, B.M., PTACEK, J.L., LAVIGNE, M., HORNER, T.J. (2019) Barium in deep-sea bamboo corals: Phase associations, barium stable isotopes, & prospects for paleoceanography. *Earth and Planetary Science Letters* 525, 115751. <https://doi.org/10.1016/j.epsl.2019.115751>
- HORNER, T.J., KINSLEY, C.W., NIELSEN, S.G. (2015) Barium-isotopic fractionation in seawater mediated by barite cycling and oceanic circulation. *Earth and Planetary Science Letters* 430, 511–522. <https://doi.org/10.1016/j.epsl.2015.07.027>
- HORNER, T.J., PRYER, H.V., NIELSEN, S.G., CROCKFORD, P.W., GAUGLITZ, J.M., WING, B.A., RICKETTS, R.D. (2017) Pelagic barite precipitation at micromolar ambient sulfate. *Nature Communications* 8, 1342. <https://doi.org/10.1038/s41467-017-01229-5>
- HSIEH, Y.-T., HENDERSON, G.M. (2017) Barium stable isotopes in the global ocean: Tracer of Ba inputs and utilization. *Earth and Planetary Science Letters* 473, 269–278. <https://doi.org/10.1016/j.epsl.2017.06.024>
- HSIEH, Y.-T., BRIDGESTOCK, L., SCHEUERMANN, P.P., SEYFRIED JR., W.E., HENDERSON, G.M. (2021) Barium isotopes in mid-ocean ridge hydrothermal vent fluids: A source of isotopically heavy Ba to the ocean. *Geochimica et Cosmochimica Acta* 292, 348–363. <https://doi.org/10.1016/j.gca.2020.09.037>
- JANSSEN, D.J., ABOUCHAMI, W., GALER, S.J.G., CULLEN, J.T. (2017) Fine-scale spatial and interannual cadmium isotope variability in the subarctic northeast Pacific. *Earth and Planetary Science Letters* 472, 241–252. <https://doi.org/10.1016/j.epsl.2017.04.048>
- LEA, D.W., BOYLE, E.A. (1991) Barium in planktonic foraminifera. *Geochimica et Cosmochimica Acta* 55, 3321–3331. [https://doi.org/10.1016/0016-7037\(91\)90491-M](https://doi.org/10.1016/0016-7037(91)90491-M)
- RAHMAN, S., SHILLER, A.M., ANDERSON, R.F., CHARETTE, M.A., HAYES, C.T., GILBERT, M., GRISSOM, K.R., LAM, P.J., OHNEMUS, D.C., PAVIA, F.J., TWINING, B.S., VIVANCOS, S.M. (2022) Dissolved and Particulate Barium Distributions Along the US GEOTRACES North Atlantic and East Pacific Zonal Transects (GA03 and GP16): Global Implications for the Marine Barium Cycle. *Global Biogeochemical Cycles* 36, e2022GB007330. <https://doi.org/10.1029/2022GB007330>
- SCHLITZER, R. (2022) *Ocean Data View*. <http://odv.awi.de>
- SCHLITZER, R., ANDERSON, R.F., DODAS, E.M., LOHAN, M., GEIBERT, W., et al. (2018) The GEOTRACES Intermediate Data Product 2017. *Chemical Geology* 493, 210–223. <https://doi.org/10.1016/j.chemgeo.2018.05.040>
- SUNDA, W.G., HUNTSMAN, S.A. (1997) Interrelated influence of iron, light and cell size on marine phytoplankton growth. *Nature* 390, 389–392. <https://doi.org/10.1038/37093>
- VAN ZUILEN, K., MÜLLER, T., NÄGLER, T.F., DIETZEL, M., KÜSTERS, T. (2016) Experimental determination of barium isotope fractionation during diffusion and adsorption processes at low temperatures. *Geochimica et Cosmochimica Acta* 186, 226–241. <https://doi.org/10.1016/j.gca.2016.04.049>
- VON ALLMEN, K., BÖTTCHER, M.E., SAMANKASSOU, E., NÄGLER, T.F. (2010) Barium isotope fractionation in the global barium cycle: First evidence from barium minerals and precipitation experiments. *Chemical Geology* 277, 70–77. <https://doi.org/10.1016/j.chemgeo.2010.07.011>
- WHITMORE, L.M., SHILLER, A.M., HORNER, T.J., XIANG, Y., AURO, M.E., BAUCH, D., DEHAIRS, F., LAM, P.J., LI, J., MALDONADO, M.T., MEARS, C., NEWTON, R., PASQUALINI, A., PLANQUETTE, H., REMBER, R., THOMAS, H. (2022) Strong Margin Influence on the Arctic Ocean Barium Cycle Revealed by Pan-Arctic Synthesis. *Journal of Geophysical Research: Oceans* 127, e2021JC017417. <https://doi.org/10.1029/2021JC017417>
- XIE, R.C., REHKÄMPER, M., GRASSE, P., VAN DE FLIEDT, T., FRANK, M., XUE, Z. (2019) Isotopic evidence for complex biogeochemical cycling of Cd in the eastern tropical South Pacific. *Earth and Planetary Science Letters* 512, 134–146. <https://doi.org/10.1016/j.epsl.2019.02.001>
- YU, Y., SIEBERT, C., FIETZKE, J., GOEPFERT, T., HATHORNE, E., CAO, Z., FRANK, M. (2020) The impact of MC-ICP-MS plasma conditions on the accuracy and precision of stable isotope measurements evaluated for barium isotopes. *Chemical Geology* 549, 119697. <https://doi.org/10.1016/j.chemgeo.2020.119697>

High Latitude Controls on Dissolved Barium Isotope Distributions in the Global Ocean

Y. Yu, R.C. Xie, M. Gutjahr, G. Laukert, Z. Cao, E.C. Hathorne, C. Siebert, G. Patton, M. Frank

Supplementary Information

The Supplementary Information includes:

- Sample Collection and Preparation
- Hydrography
- Laboratory Analyses and Results
- Regeneration Model
- Conservative Mixing Model
- Estimation of the Net Accumulated $\delta^{138}\text{Ba}$ Signal in the North Pacific
- Supplementary Table S-1
- Supplementary Figures S-1 to S-3
- Supplementary Information References

Sample Collection and Preparation

The seawater samples analysed in this study were collected from the Fram Strait (Nordic Seas), the Labrador Sea, the Weddell Sea, and the Pacific Ocean. The Fram Strait seawater samples were acquired along the 78.8 °N meridional transect during expedition PS80 of the German research vessel RV *Polarstern* between 15 June and 15 July 2012 (Beszczynska-Möller and Wisotzki, 2012). For Ba concentration and isotope measurements, aliquots of the filtered (0.45 µm, filtration with Millipore® cellulose acetate filters) and acidified (pH ≈ 2, on board acidification with concentrated distilled HCl) samples were selected from four full water column stations down to a maximum depth of 2668 m. More information on sample collection, hydrography and CTD (conductivity, temperature, depth) profiles are available from Laukert *et al.* (2017). Aliquots of filtered (0.2 µm, direct filtration with PALL filters) and acidified (same pH and procedure as for the Fram Strait samples) seawater samples from the Labrador Sea were chosen from four stations conducted during the cruise MSM39 and the cruise MSM45 PULSE (Paleoclimate Understanding Labrador Sea) of the German research vessel RV *Maria S. Merian* in June 2014 and August 2015 (Schneider *et al.*, 2016). Aliquots of the Weddell Sea samples (filtered and acidified in the same manner as the Labrador Sea samples) were picked from four full depth profiles in the southern and western Weddell Sea during the two expeditions PS111 and PS118 of the German research vessel RV *Polarstern* in 2018 and 2019. Further details on sampling and hydrographic conditions are available from the cruise reports of PS111 and PS118 (Schröder, 2018; Dorschel, 2019). Aliquots of the Pacific samples (filtered

and acidified in the same manner as the Labrador Sea samples) were picked from five depth profiles in the South and North Pacific during the expedition SO264 of the German research vessel RV *Sonne* in 2018 (Nürnberg, 2018). More information on sample collection, hydrography and CTD (conductivity, temperature, depth) profiles are available from Fuhr *et al.* (2021).

Hydrography

Figure S-1 provides a *T-S* diagram for all deep water masses encountered in this study contoured by potential density. The measured Ba concentrations ([Ba]) and isotope compositions ($\delta^{138}\text{Ba}$) for all water samples are presented in Table S-1 with their hydrographic properties and water masses. In the Nordic Seas, the East Greenland Current (EGC) transports cold and fresh shallow waters exiting the Arctic Ocean and Atlantic Water (AW) recirculating in the Fram Strait or in the Arctic Ocean across the Greenland Scotland Ridge (GSR) forming a part of the Nordic Seas overflows (Dickson *et al.*, 1990). Once the Northern Overflow Water (NOW) has crossed the GSR as the Denmark Strait Overflow Water (DSOW) and the Iceland Scotland Overflow Water (ISOW), they descend and subsequently entrain intermediate waters present in the Irminger and Iceland Basins, such as Labrador Sea Water (LSW) and Subpolar Mode Water (SPMW). This process forms Northwest Atlantic Bottom Water (NWABW) and Northeast Atlantic Deep Water (NEADW; Dickson and Brown, 1994). Thereafter, NWABW and NEADW merge south of the Denmark Strait forming the upper and lower branches of the Deep Western Boundary Current (DWBC) when reaching Cape Farewell. The DWBC subsequently flows into the Labrador Basin and mixes with LSW thereby forming North Atlantic Deep Water (NADW), which constitutes the northern-deep limb of the Atlantic meridional overturning circulation (AMOC; Dickson and Brown, 1994; Yashayaev, 2007). In the Southern Ocean, the circulation regime is dominated by the eastward flowing Antarctic Circumpolar Current (ACC) and the cyclonically circulating Weddell Gyre (WG) that is located between the southern boundary of the ACC and the Antarctic shelf of the Weddell Sea (Fahrbach *et al.*, 1994). The two major source waters that contribute to the formation of Antarctic Bottom Water (AABW) are warm remnants of the regional Circumpolar Deep Water (CDW) that have been imported from the ACC, and the extremely cold and dense shelf waters resulting from brine rejection during sea-ice formation (Orsi *et al.*, 1999). Part of this mixture that is dense enough to reach the bottom forms Weddell Sea Bottom Water (WSBW), which is, however, too dense to escape from the Weddell Basin (Stichel *et al.*, 2012). Only the less dense part of the mixture can feed into Weddell Sea Deep Water (WSDW), which leaves the Weddell Basin via deep gaps across the South Scotia Ridge and becomes the major contributor to AABW constituting the southern-deep limb of the AMOC (Orsi *et al.*, 1999). The deep-water circulation in the North Pacific is mainly driven by density gradients and is characterised by the advection and mixing of Lower and Upper Circumpolar Deep Water (LCDW/UCDW) and North Pacific Deep Water (NPDW). The UCDW initially follows the Antarctic Intermediate Water (AAIW) at greater depths but takes a more north-westerly path into the Caroline Basin and further into the Philippine Sea where it eventually upwells (Kawabe and Fujio, 2010).

Laboratory Analyses and Results

The dissolved seawater Ba concentrations ([Ba]) were analysed applying an isotope dilution technique with an Agilent 7500ce inductively coupled plasma mass spectrometer (ICP-MS) at GEOMAR, Kiel. Briefly, an aliquot (50 μL) of acidified seawater was accurately weighed and mixed with defined amounts of an ^{135}Ba single spike to achieve a $^{138}\text{Ba}/^{135}\text{Ba}$ ratio near 0.64. The spike-equilibrated samples were then diluted to about 500 μL with 2 % HNO_3 before the $^{138}\text{Ba}/^{135}\text{Ba}$ ratios were measured and mass bias corrected by bracketing analyses of a natural Ba standard solution. Depending on Ba concentration, aliquots of 5 mL ($>60 \text{ nmol kg}^{-1}$) or 10 mL ($<60 \text{ nmol kg}^{-1}$) of the seawater samples were appropriately spiked with an ^{130}Ba - ^{135}Ba double spike. After an equilibration period of 24 hours, Ba was co-precipitated with CaCO_3 and the resulting precipitates were centrifuged and dissolved in 2 mL of 1 M HCl in preparation



for cation exchange chromatography. Samples were twice passed through columns containing 1.4 mL of Bio-Rad AG 50W-X8 (200–400 mesh size) resin. Matrix elements were subsequently eluted with 8 mL of 1 M HCl and 8 mL of 3 M HCl, respectively. The Ba cuts were then collected with 10 mL of 2 M HNO₃, dried and re-dissolved in 2 % (v/v) HNO₃ for Ba isotope analyses. Stable Ba isotope measurements were performed with a Thermo Fisher Neptune Plus MC-ICP-MS at GEOMAR, Kiel. The analyte was introduced as a dry aerosol using an Aridus II desolvating system (CETAC Technologies, Omaha, NE, USA) and an Aspire PFA micro-concentric nebuliser (uptake rate of ~ 50 µL min⁻¹). The MC-ICP-MS was tuned to a matrix tolerance state defined by a high Normalised Argon Index value (NAI, an index of plasma temperature; Yu *et al.* 2020). A three-dimensional data reduction procedure following Siebert *et al.* (2001) was used to correct for both instrumental and natural mass-dependent isotope fractionation. The Ba isotope compositions are reported in per mil (‰) relative to the National Institute of Standards and Technology (NIST) SRM 3014a Ba standard ($\delta^{138}\text{Ba} = {}^{138}/{}^{134}\text{Ba}_{\text{sample}}/{}^{138}/{}^{134}\text{Ba}_{\text{NIST}} - 1$). The uncertainty is reported as the larger of either the internal 2 standard error (2 s.e.) of repeated sample measurements or the long-term 2 s.d. reproducibility (± 0.04 ‰) of repeated SAFe 1000 m measurements.

The depth profiles of [Ba] and $\delta^{138}\text{Ba}$ are shown in Figure S-2. In the Fram Strait, the depth profiles of [Ba] and $\delta^{138}\text{Ba}$ are similar for all four stations in that Ba is modestly depleted in surface waters associated with relatively heavy $\delta^{138}\text{Ba}$ values of 0.52 ‰. With increasing depth from 200 m to the bottom, [Ba] generally increases from 43 to 49 nmol kg⁻¹ and $\delta^{138}\text{Ba}$ values slightly decrease from 0.52 to 0.46 ‰. In the Labrador Sea, the vertical distributions of $\delta^{138}\text{Ba}$ and [Ba] are similar to those of the Fram Strait and only display little variability along the cyclonic circulation within the Labrador Basin. Dissolved [Ba] exhibits moderate depletion at the surface and relative enrichment at depth, resembling nutrient-type depth profiles and mirroring the $\delta^{138}\text{Ba}$ profiles. All depth profile samples below 1000 m water depth, where NADW dominates (Dickson and Brown, 1994), feature an average $\delta^{138}\text{Ba}$ value of 0.48 ‰ and an average [Ba] value of 50 nmol kg⁻¹. In the Weddell Sea, the depth profiles show slight enrichments towards heavy isotopic compositions in the surface layer relative to deeper waters, which are associated with lower [Ba] values. The nature of the vertical gradient in $\delta^{138}\text{Ba}$ and its relationship to [Ba] varies insignificantly with sampling sites along the WG, as well as with water depth. Such a vertical distribution is also consistent with the pattern reported for St. Super5 at the north rim of the WG (Fig. S-2; Hsieh and Henderson, 2017). At depths between 2000 and 4000 m, where the water masses are dominated by WSDW/AABW (Orsi *et al.*, 1999), dissolved [Ba] and $\delta^{138}\text{Ba}$ are constrained to average values of 99 nmol kg⁻¹ and 0.26 ‰, respectively. In the Pacific Ocean, surface and sub-surface waters are characterised by higher $\delta^{138}\text{Ba}$ values than those from the Atlantic Ocean. The deep-water masses (below 2000 m) are characterised by Ba isotope compositions indistinguishable from those of the deep Weddell Sea but significantly higher [Ba]. In the tropical South Pacific, LCDW exhibits a $\delta^{138}\text{Ba}$ value of 0.28 ‰ and a [Ba] value of 120 nmol kg⁻¹, while NPDW is characterised by a $\delta^{138}\text{Ba}$ value of 0.25 ‰ and a [Ba] value of 160 nmol kg⁻¹ in the high-latitude North Pacific.

Regeneration Model

A regeneration model has been applied to explain the relationship between dissolved $\delta^{138}\text{Ba}$ and [Ba] in seawater samples. Based on isotope mass balance, the continuous addition of Ba to deep waters by dissolution of sinking particles causes systematic changes in $\delta^{138}\text{Ba}$ and [Ba]. In this case, the following equation can be applied following the method from Bridgestock *et al.* (2018):

$$\delta^{138}\text{Ba} = (\delta^{138}\text{Ba}_{\text{pre}} \times f_{\text{pre}}) + (\delta^{138}\text{Ba}_{\text{regen}} \times f_{\text{regen}}), \quad (\text{Eq. S-1})$$

where $\delta^{138}\text{Ba}_{\text{pre}}$ and $\delta^{138}\text{Ba}_{\text{regen}}$ denote the Ba isotope composition of the preformed and the regenerated fractions, respectively. f_{pre} and f_{regen} denote the fraction of the Ba from the preformed and regenerated reservoirs, respectively ($f_{\text{pre}} + f_{\text{regen}} = 1$). If there is no isotope fractionation accompanying Ba regeneration, this model assumes that increases in [Ba] and associated decreases in $\delta^{138}\text{Ba}$ with depth are purely controlled by the addition of Ba from sinking particles.



Assuming [Ba] and $\delta^{138}\text{Ba}$ value of 35 nmol kg^{-1} and 0.62 ‰ represents the preformed signals with a characterised sinking particles $\delta^{138}\text{Ba}$ value of 0.10 ‰ (Horner *et al.*, 2017; Bridgestock *et al.*, 2018), the regeneration model defines a linear correlation in a plot of $\delta^{138}\text{Ba}$ against $1/[\text{Ba}]$, which gradually deviates from the mixing relationship at higher [Ba] (Fig. 4).

Conservative Mixing Model

A conservative mixing model has been applied by using salinity (S) as a conservative tracer to quantify the variability of dissolved Ba isotopes ($\delta^{138}\text{Ba}$) not related to conservative mixing in the low and mid-latitude Atlantic and Pacific Ocean. The conservative mixing model is described by:

$$S_{\text{mix}} = S_a \times f_a + S_b \times f_b, \quad (\text{Eq. S-2})$$

$$\delta^{138}\text{Ba}_{\text{mix}} = ([\text{Ba}]_a \times \delta^{138}\text{Ba}_a \times f_a + [\text{Ba}]_b \times \delta^{138}\text{Ba}_b \times f_b) / ([\text{Ba}]_a \times f_a + [\text{Ba}]_b \times f_b), \quad (\text{Eq. S-3})$$

where mix, a and b denote the components of the mixed and a and b endmember water masses, respectively. The factors f_a and f_b denote the fractional contributions of the two endmember water masses ($f_a + f_b = 1$). For mixing calculations in the deep Atlantic, NADW ($S = 35.00$, $\delta^{138}\text{Ba} = 0.48 \text{ ‰}$, $[\text{Ba}] = 50 \text{ nmol kg}^{-1}$) and AABW ($S = 34.70$, $\delta^{138}\text{Ba} = 0.26 \text{ ‰}$, $[\text{Ba}] = 99 \text{ nmol kg}^{-1}$) were used as simplified water mass endmembers. For mixing calculations in the deep Pacific, LCDW ($S = 34.70$, $\delta^{138}\text{Ba} = 0.28 \text{ ‰}$, $[\text{Ba}] = 120 \text{ nmol kg}^{-1}$) and NPDW ($S = 34.60$, $\delta^{138}\text{Ba} = 0.25 \text{ ‰}$, $[\text{Ba}] = 160 \text{ nmol kg}^{-1}$) were used as simplified water mass endmembers. Deviations from conservative mixing exceeding 0.04 ‰ indicate non-conservative behaviour, based on the 2 s.d. uncertainty of the Ba isotope measurements carried out at GEOMAR. As shown in Figure S-3, the signatures of all water samples below 2000 m from the low and mid-latitude deep Atlantic and Pacific do not deviate from the mixing lines in both ocean basins taking into account the analytical uncertainty of the Ba isotope measurements.

Estimation of the Net Accumulated $\delta^{138}\text{Ba}$ Signal in the North Pacific

A 34 % increase in deep water [Ba] from the Southern Ocean to the North Pacific, without a corresponding variation in $\delta^{138}\text{Ba}$, puts constraints on the Ba isotope compositions of the net accumulated dissolved Ba from remineralisation of sinking particles in the North Pacific. A simple mass balance calculation developed for stable Cd isotopes by Janssen *et al.* (2017) is applied to estimate the accumulated $\delta^{138}\text{Ba}$ signal in the North Pacific:

$$[\text{Ba}]_{\text{SO}} + [\text{Ba}]_{\text{acm}} = [\text{Ba}]_{\text{Pac}}, \quad (\text{Eq. S-4})$$

$$[\text{Ba}]_{\text{SO}} \times \delta^{138}\text{Ba}_{\text{SO}} + [\text{Ba}]_{\text{acm}} \times \delta^{138}\text{Ba}_{\text{acm}} = [\text{Ba}]_{\text{Pac}} \times \delta^{138}\text{Ba}_{\text{Pac}}, \quad (\text{Eq. S-5})$$

where $[\text{Ba}]_{\text{SO}}$, $[\text{Ba}]_{\text{acm}}$ and $[\text{Ba}]_{\text{Pac}}$ denote the Ba concentrations of the deep Southern Ocean, the accumulated fraction and the deep North Pacific, respectively. $\delta^{138}\text{Ba}_{\text{SO}}$, $\delta^{138}\text{Ba}_{\text{acm}}$ and $\delta^{138}\text{Ba}_{\text{Pac}}$ denote the Ba isotope compositions of the deep Southern Ocean, the accumulated fraction and the deep North Pacific, respectively. Using the arithmetic mean of deep water $\delta^{138}\text{Ba}$ from each water mass and the 2 s.d. error on this mean, the net accumulated Ba in the deep North Pacific is characterised by an average $\delta^{138}\text{Ba}_{\text{acm}}$ value of $0.22 \pm 0.24 \text{ ‰}$.



Supplementary Table

Table S-1 Detailed data for the seawater samples from this study.

Table S-1 (.xlsx) can be downloaded from the online version of this article at <https://doi.org/10.7185/geochemlet.2242>.

Supplementary Figures

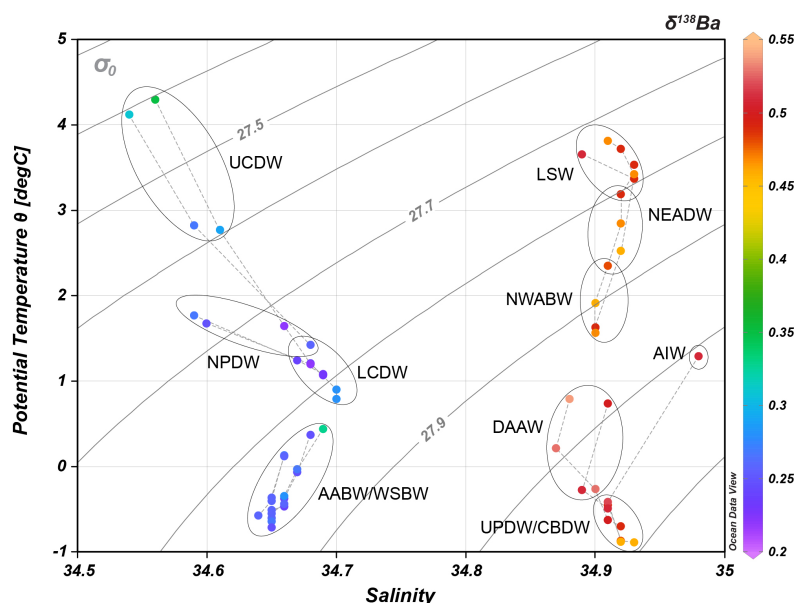


Figure S-1 *T-S* diagram for all deep water masses encountered in this study contoured by potential density. The water masses are marked with circles. Colours indicate the dissolved Ba isotope compositions ($\delta^{138}\text{Ba}$). UCDW, Upper Circumpolar Deep Water; NPDW, North Pacific Deep Water; LCDW, Lower Circumpolar Deep Water; AABW, Antarctic Bottom Water; WSBW, Weddell Sea Bottom Water; LSW, Labrador Sea Water; NEADW, Northeast Atlantic Deep Water; NWABW, Northwest Atlantic Bottom Water; AIW, Arctic Intermediate Water; DAAW, Dense Arctic Atlantic Water; UPDW, Upper Polar Deep Water; CBDW, Canadian Basin Deep Water. Figure was produced using Ocean Data View (Schlitzer, 2022) and modified manually.

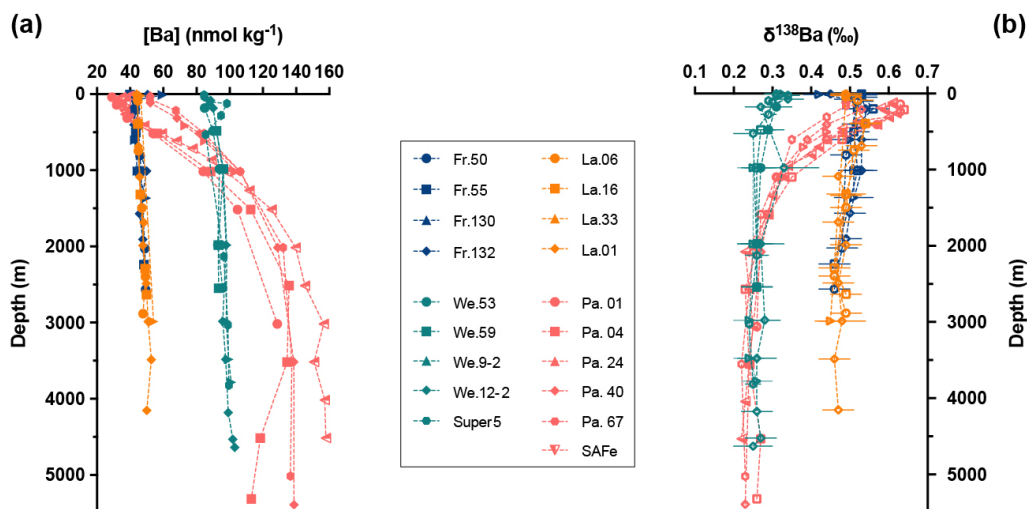


Figure S-2 Depth profiles of the (a) dissolved Ba concentrations and (b) isotope compositions in the Fram Strait (blue), the Labrador Sea (orange), the Weddell Sea (green) and the Pacific Ocean (pink). The error bars for $\delta^{138}\text{Ba}$ are the larger of either the internal 2 s.e. of repeated sample measurements or the long-term 2 s.d. reproducibility (± 0.04 ‰) of repeated SAFE (1000 m) measurements. Data for station Super5 and SAFE are from Hsieh and Henderson (2017) and Geyman *et al.* (2019), respectively.

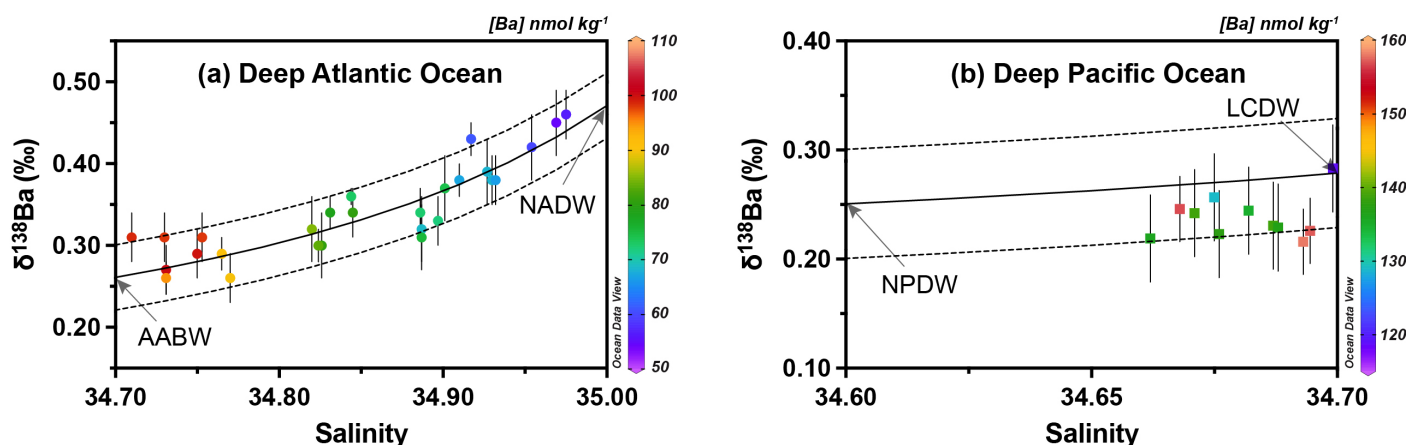


Figure S-3 Salinity versus $\delta^{138}\text{Ba}$ diagrams for deep water masses of the (a) Atlantic and (b) Pacific Ocean below 2000 m water depth; colours denote dissolved [Ba]. All measured $\delta^{138}\text{Ba}$ values from the low and mid-latitude oceans are consistent within analytical error with the conservative mixing curves and their 0.04 ‰ uncertainty range (dashed curves). NADW, North Atlantic Deep Water; AABW, Antarctic Bottom Water; LCDW, Lower Circumpolar Deep Water; NPDW, North Pacific Deep Water. Figures were produced using Ocean Data View (Schlitzer, 2022) and modified manually.

Supplementary Information References

- Beszczynska-Möller, A., Wisotzki, A. (2012) *Physical oceanography during POLARSTERN cruise ARK-XXVII/1*. Alfred Wegener Institute, Helmholtz Centre for Polar and Marine Research, Bremerhaven; PANGAEA. <https://doi.org/10.1594/PANGAEA.801791>
- Bridgestock, L., Hsieh, Y.-T., Porcelli, D., Homoky, W.B., Bryan, A., Henderson, G.M. (2018) Controls on the barium isotope compositions of marine sediments. *Earth and Planetary Science Letters* 481, 101–110. <https://doi.org/10.1016/j.epsl.2017.10.019>
- Dickson, R.R., Brown, J. (1994) The production of North Atlantic Deep Water: Sources, rates, and pathways. *Journal of Geophysical Research: Oceans* 99, 12319–12341. <https://doi.org/10.1029/94JC00530>
- Dickson, R.R., Gmitrowicz, E.M., Watson, A.J. (1990) Deep-water renewal in the northern North Atlantic. *Nature* 344, 848–850. <https://doi.org/10.1038/344848a0>
- Dorschel, B. (2019) The Expedition PS118 of the Research Vessel POLARSTERN to the Weddell Sea in 2019. *Reports on Polar and Marine Research* 735, Alfred-Wegener-Institut, Helmholtz-Zentrum für Polar- und Meeresforschung, Bremerhaven, Germany, 149 pp. https://doi.org/10.2312/BzPM_0735_2019
- Fahrbach, E., Rohardt, G., Schröder, M., Strass, V. (1994) Transport and structure of the Weddell Gyre. *Annales Geophysicae* 12, 840–855. <https://doi.org/10.1007/s00585-994-0840-7>
- Fuhr, M., Laukert, G., Yu, Y., Nürnberg, D., Frank, M. (2021) Tracing Water Mass Mixing from the Equatorial to the North Pacific Ocean with Dissolved Neodymium Isotopes and Concentrations. *Frontiers in Marine Science* 7, 603761. <https://doi.org/10.3389/fmars.2020.603761>
- Geyman, B.M., Ptacek, J.L., LaVigne, M., Horner, T.J. (2019) Barium in deep-sea bamboo corals: Phase associations, barium stable isotopes, & prospects for paleoceanography. *Earth and Planetary Science Letters* 525, 115751. <https://doi.org/10.1016/j.epsl.2019.115751>
- Horner, T.J., Pryer, H.V., Nielsen, S.G., Crockford, P.W., Gauglitz, J.M., Wing, B.A., Ricketts, R.D. (2017) Pelagic barite precipitation at micromolar ambient sulfate. *Nature Communications* 8, 1342. <https://doi.org/10.1038/s41467-017-01229-5>
- Hsieh, Y.-T., Henderson, G.M. (2017) Barium stable isotopes in the global ocean: Tracer of Ba inputs and utilization. *Earth and Planetary Science Letters* 473, 269–278. <https://doi.org/10.1016/j.epsl.2017.06.024>
- Janssen, D.J., Abouchami, W., Galer, S.J.G., Cullen, J.T. (2017) Fine-scale spatial and interannual cadmium isotope variability in the subarctic northeast Pacific. *Earth and Planetary Science Letters* 472, 241–252. <https://doi.org/10.1016/j.epsl.2017.04.048>
- Kawabe, M., Fujio, S. (2010) Pacific ocean circulation based on observation. *Journal of Oceanography* 66, 389–403. <https://doi.org/10.1007/s10872-010-0034-8>
- Laukert, G., Frank, M., Bauch, D., Hathorne, E.C., Rabe, B., von Appen, W.-J., Wegner, C., Zieringer, M., Kassens, H. (2017) Ocean circulation and freshwater pathways in the Arctic Mediterranean based on a combined Nd isotope, REE and oxygen isotope section across Fram Strait. *Geochimica et Cosmochimica Acta* 202, 285–309. <https://doi.org/10.1016/j.gca.2016.12.028>
- Nürnberg, D. (Ed.) (2018) *RV SONNE Fahrtbericht / Cruise Report SO264-SONNE-EMPEROR: The Plio/Pleistocene to Holocene development of the pelagic North Pacific from surface to depth – assessing its role for the global carbon budget and Earth's climate, Suva (Fiji) – Yokohama (Japan), 30.6. – 24.8.2018*. GEOMAR Helmholtz-Zentrum für Ozeanforschung, Kiel, Germany, 284 pp. https://doi.org/10.3289/GEOMAR_REP_NS_46_2018
- Orsi, A.H., Johnson, G.C., Bullister, J.L. (1999) Circulation, mixing, and production of Antarctic Bottom Water. *Progress in Oceanography* 43, 55–109. [https://doi.org/10.1016/S0079-6611\(99\)00004-X](https://doi.org/10.1016/S0079-6611(99)00004-X)
- Schlitzer, R. (2022) Ocean Data View. <http://odv.awi.de>
- Schneider, R.R., Blanz, T., Evers, F., Gasparotto, M.-C., Gross, F., Hüls, M., Keul, N., Kienast, M., Lehner, K., Lüders, S., Mellon, S., Merl, M., Reissig, S., Repschläger, J., Salvatelli, R., Schulten, I., Schwarz, J.-P., Schönke, M., Steen, E., Tietjens, A., Van Nieuwenhove, N. (2016) Paleoclimate Understanding Labrador Sea (PULSE), Cruise No. MSM45, August 1, 2015 - August 21, 2015, Nuuk (Greenland) - Halifax (Canada). *MARIA S. MERIAN-Berichte MSM45*, Gutachterpanel Forschungsschiffe, Bonn, Germany, 38 pp. https://doi.org/10.2312/cr_msm45



- Schröder, M. (2018) The Expedition PS111 of the Research Vessel POLARSTERN to the southern Weddell Sea in 2018. *Reports on Polar and Marine Research* 718, Alfred-Wegener-Institut, Helmholtz-Zentrum für Polar- und Meeresforschung, Bremerhaven, Germany, 161 pp. https://doi.org/10.2312/BzPM_0718_2018
- Siebert, C., Nögler, T.F., Kramers, J.D. (2001) Determination of molybdenum isotope fractionation by double-spike multicollector inductively coupled plasma mass spectrometry. *Geochemistry, Geophysics, Geosystems* 2, 2000GC000124. <https://doi.org/10.1029/2000GC000124>
- Stichel, T., Frank, M., Rickli, J., Hathorne, E.C., Haley, B.A., Jeandel, C., Pradoux, C. (2012) Sources and input mechanisms of hafnium and neodymium in surface waters of the Atlantic sector of the Southern Ocean. *Geochimica et Cosmochimica Acta* 94, 22–37. <https://doi.org/10.1016/j.gca.2012.07.005>
- Yashayaev, I. (2007) Hydrographic changes in the Labrador Sea, 1960–2005. *Progress in Oceanography* 73, 242–276. <https://doi.org/10.1016/j.pocean.2007.04.015>
- Yu, Y., Siebert, C., Fietzke, J., Goepfert, T., Hathorne, E., Cao, Z., Frank, M. (2020) The impact of MC-ICP-MS plasma conditions on the accuracy and precision of stable isotope measurements evaluated for barium isotopes. *Chemical Geology* 549, 119697. <https://doi.org/10.1016/j.chemgeo.2020.119697>